Hindawi Publishing Corporation
International Journal of Antennas and Propagation
Volume 2014, Article ID 392895, 12 pages
http://dx.doi.org/10.1155/2014/392895

Research Article

Direction Finding Using Multiple Sum and Difference Patterns in 4D Antenna Arrays

Quanjiang Zhu, Shiwen Yang, Ruilin Yao, and Zaiping Nie

School of Electronic Engineering, University of Electronic Science and Technology of China (UESTC), Chengdu 611731, China

Correspondence should be addressed to Shiwen Yang; swnyang@uestc.edu.cn

Received 4 January 2014; Accepted 19 March 2014; Published 21 May 2014

Academic Editor: Paolo Rocca

Traditional monopulse systems used for direction finding usually face the contradiction between high angle precision and wide angle-searching field, and a compromise has to be made. In this paper, the time modulation technique in four-dimensional (4D) antenna array is introduced into the conventional phase-comparison monopulse to form a novel direction-finding system, in which both high angle resolution and wide field-of-view are realized. The full 4D array is divided into two subarrays and the differential evolution (DE) algorithm is used to optimize the time sequence of each subarray to generate multibeams at the center frequency and low sidebands. Then the multibeams of the two subarrays are phase-compared with each other and multiple pairs of sum-difference beams are formed at different sidebands and point to different spatial angles. The proposed direction-finding system covers a large field-of-view of up to ±60° and simultaneously maintains the advantages of monopulse systems, such as high angle precision and low computation complexity. Theoretical analysis and experimental results validate the effectiveness of the proposed system.

1. Introduction

Monopulse systems, which were evolved from sequential lobing, are capable of eliminating the errors caused by amplitude fluctuations of target echoes and increase the data rate, since that angle information can be derived from a single pulse [1]. Monopulse has great advantages, such as very high angular precision and very low computational complexity and has been used in many applications, such as air traffic control, missile tracking, and space antennas. A classic and simple type of monopulse is the phase-comparison monopulse, which uses the measured phase differences of two antennas' outputs to establish the target bearing. An inherent problem with such monopulse system is that the resulting angle information can be ambiguous when the spacing of the two antennas or arrays is more than half a wavelength, which is often the case for high precision measurement [2, 3]. One of the common ways to solve this ambiguity problem is to use staggered baseline length [3, 4], which is to make another measurement with a different antenna spacing (and thus different ambiguity) and combine the two ambiguous measurements into one unambiguous measurement. Other ambiguity resolution techniques include the use of multiple frequencies, baseline rotation or frequency modulation, and so forth. However, these methods either require extra antenna element, receiver electronics and additional installation space, or require the increased complexity or computation time.

As compared to the aforementioned techniques, the four-dimensional (4D) antenna array provides another method to resolve the multiple ambiguities. The 4D antenna array uses time as the fourth design parameter to alleviate the stringent requirement on traditional antenna arrays operating in the 3D space, which is realized by time-modulating the antenna arrays with high speed RF switches. Since its inception in the 1959 [5], many researchers have paid great attention to this novel technology, especially during the past decade [6–19]. As a result of time modulation in 4D arrays, sidebands are generated at multiples of the time modulation frequency. These sideband signals can either be suppressed or be enhanced through the optimization of the exciting time sequences [7–13]. In [14], the sidebands were purposely utilized and a two-element 4D array was configured to operate as a direction-finding system, in which the sum

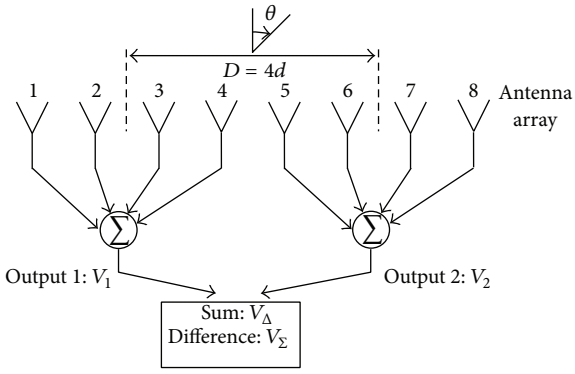

Figure 1: A phase-comparison monopulse system based on a conventional 8-element array.

pattern was formed at the center frequency and the difference pattern was formed at the first sideband. Relevant experiment was then conducted in [15], and the measured results confirmed the theoretical analysis. Some monopulse systems based on the 4D arrays have been conceptually designed and numerically verified [16–19]. However, the contradiction between precise angle estimation and large field-of-view was not addressed in these papers. In [20], the time modulation technique in 4D arrays was firstly proposed as a method of resolving the ambiguities existing in phase-comparison monopulse systems. However, no experiment is performed to validate the idea, and the signal processing units are not addressed.

In this paper, a novel phase-comparison monopulse based on the 4D antenna array is presented. The sidebands of a 4D antenna array are enhanced and utilized not only to generate multiple beams but also to resolve the multiple ambiguities. The proposed technique makes it possible to realize unambiguous high accuracy direction finding over a large field-of-view of more than ±60°. This paper is organized as follows. In Section 2, the conventional phase-comparison monopulse and the 4D arrays are introduced. In Section 3, the novel monopulse system based on a 4D array is presented and its working principle is analyzed. In Section 4, an experimental system composed of 4D arrays is built, and the experimental results and corresponding signal processing steps are presented in detail. Finally, some conclusions are drawn.

2. Theoretical Backgrounds

2.1. Conventional Phase-Comparison Monopulse. There are two types of monopulse systems, namely, amplitude-comparison monopulse and phase-comparison monopulse. The phase-comparison monopulse is defined in terms of receiving beams with different phase centers [1] and is adopted as the type of monopulse in this paper.

As illustrated in Figure 1, an array model with 8 isotropic elements is used to demonstrate the basic principles of phase-comparison monopulse. The full array is divided into two subarrays. When a plane wave impinges on the array with an angle θ measured from broadside, the received signals or voltages of the two subarrays can be written as

$$V_1 = E_0 \sum_{k=1}^{4} e^{j(k-1)\beta d \sin\theta},$$
$$V_2 = E_0 \sum_{k=1}^{4} e^{j(k-1)\beta d \sin\theta} e^{j\beta D \sin\theta}, \quad (1)$$

where E_0 is the received signal voltage of a single element, d is the element space, $D = 4d$ is the subarray distance, and β refers to the free space wave number at the operating frequency f_0. It can be seen that the received signals of the two subarrays have the same amplitude, and the only difference is the phase response. The phase difference of the two signals with respect to the center of the array equals $\beta D \sin\theta$, which is directly related to the direction of coming wave.

The sum and difference of the two received signals are given as:

$$V_\Sigma = V_2 + V_1, \quad V_\Delta = V_2 - V_1. \quad (2)$$

The difference-sum ratio between the two received signals, K, is defined as

$$K = \frac{V_\Delta}{V_\Sigma} = \frac{E_0 \sum_{k=1}^{4} e^{j(k-1)\beta d \sin\theta} \left(e^{j\beta D \sin\theta} - 1\right)}{E_0 \sum_{k=1}^{4} e^{j(k-1)\beta d \sin\theta} \left(e^{j\beta D \sin\theta} + 1\right)} = j \tan\left(\frac{\beta D}{2} \sin\theta\right). \quad (3)$$

Equation (3) is the basic direction-finding equation, which relates the difference-sum ratio K to the bearing angle θ, with the distance of the two subarray D as the parameter. The relationship among the three parameters K, θ, and D is presented in Figure 2. As can be seen from Figures 2(a)–2(d), ambiguity resolution is required as long as the subarray distance $D = 4d$ is greater than half a wavelength. In fact, since tangent and sine functions are both periodic functions, any θ that satisfies

$$\sin\theta = \frac{2\left[\arctan\left(-jK\right) \pm n\pi\right]}{\beta D} \quad \text{for } n = 0, 1, 2, \ldots \quad (4)$$

is a valid solution for (3).

As the distance D between the subarrays becomes larger, the slope of the difference-sum ratio K becomes steeper and more zeros and poles are formed. For the instance of $D = 2\lambda$ (shown in Figure 2(d)), the slope of K is the steepest of the four cases (meaning the highest measurement accuracy), and three zeros ($\theta = -30°$, 0°, and 30°) and four poles ($\theta = -48°$, $-14°$, 14°, and 48°) are formed. For any particular value of K, four ambiguous bearing angles θ correspond to it. If the angle-searching range is inside the field from $-14°$ to 14°, it is easy to determine the angle θ as K is monotonic inside this small field. However, it turns to be difficult when the searching range is beyond the field, due to ambiguity problem.

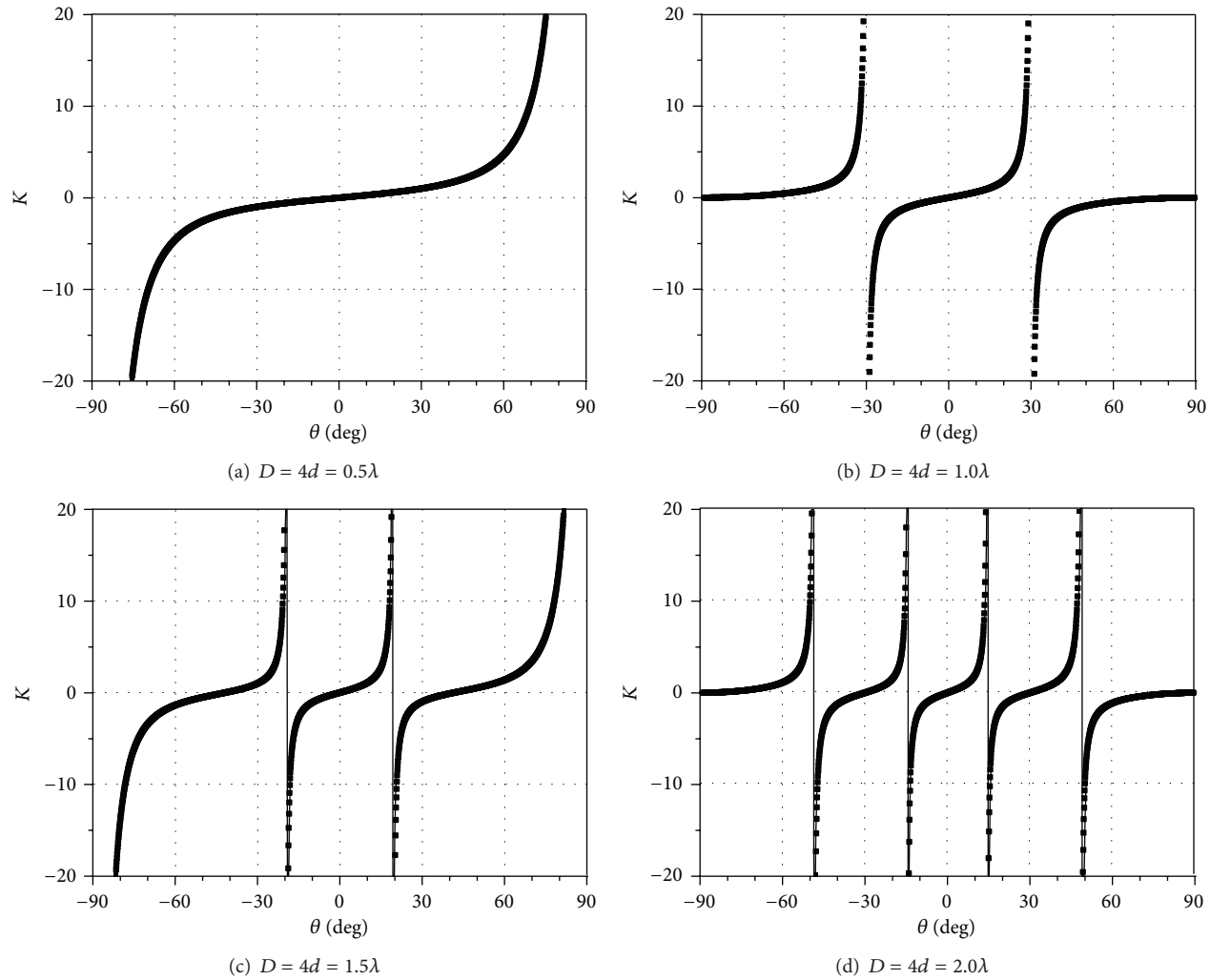

(a) $D = 4d = 0.5\lambda$

(b) $D = 4d = 1.0\lambda$

(c) $D = 4d = 1.5\lambda$

(d) $D = 4d = 2.0\lambda$

Figure 2: Difference-sum ratio K for different subarray distance.

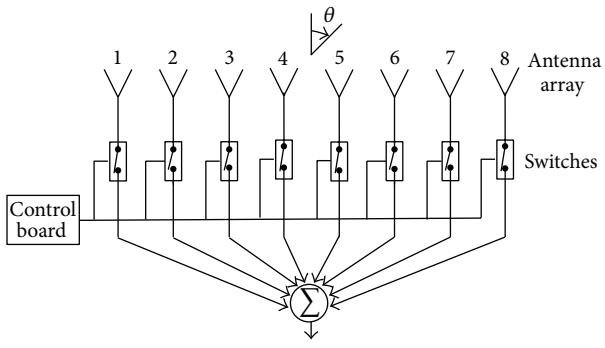

Figure 3: Block diagram of an 8-element 4D antenna array.

2.2. 4D Antenna Arrays. Unlike conventional arrays operating in 3-dimentional (3D) space, the 4D antenna arrays are formed by introducing a fourth dimension, time, into the array design, which can be realized by time-modulating conventional arrays with RF switches. Figure 3 shows the basic topology of an 8-element 4D antenna array at the receiving mode. The 4D linear array consists of 8 isotropic elements with an equal element space d. The received signal of each antenna element is time-modulated by the high speed RF switch and then summed to form the output. The RF switch is controlled by the circuit board programmed for specific time sequences. Compared with the conventional arrays, the RF switches have the effects of amplitude and phase weighting by the control of on-off state of each antenna element [21].

For a plane wave with a frequency of f_0 and the incident angle of θ with respect to the broadside of the array, the array factor of the 4D array can be given as

$$E(\theta) = e^{j2\pi f_0 t} \sum_{k=1}^{N=8} U_k(t)\, e^{j(k-1)\beta d \sin\theta}, \tag{5}$$

where $U_k(t)$ represents the periodic "on-off" state of the kth element with a time period of T_p. For different time modulation schemes, $U_k(t)$ has different forms of expression.

In this paper, the time modulation scheme of pulse shifting proposed in [22] is adopted. Accordingly, $U_k(t)$ is given by

$$U_k(t) = \begin{cases} 1 & t_k \le t \le t_k + \tau_k \\ 0 & \text{others,} \end{cases} \quad 0 \le t_k, \tau_k \le 1, \tag{6}$$

where t_k and τ_k represent the normalized switch-on instant and switch-on duration for the kth element, respectively.

Equation (5) differs from the array factor (1) of a conventional array by the time factor $U_k(t)$. As $U_k(t)$ is a periodic function with the time modulation period T_p, $U_k(t)$ can be decomposed into a Fourier series, given by [22]

$$U_k(t) = \sum_{m=-\infty}^{+\infty} a_{mk}\, e^{j2\pi m f_p t}, \tag{7}$$

$$a_{mk} = \tau_k \mathrm{sinc}\left(\pi m \tau_k\right) e^{-j\pi m(2t_k+\tau_k)}, \tag{8}$$

where a_{mk} represents the complex excitation weighting for the kth element at the mth sideband and $f_p = 1/T_p$ is the time modulation frequency. Taking into account (5) and (7), (4) can be rewritten as

$$E(\theta) = \sum_{m=-\infty}^{+\infty} e^{j2\pi(f_0 + m\, f_p)t} \sum_{k=1}^{N=8} a_{mk} e^{j(k-1)\beta d \sin\theta}, \tag{9}$$

and $E(\theta)$ can be viewed as a superposition of multiple patterns at multiple frequencies separated by the time modulation frequency f_p and is analogous to the array factors of conventional arrays.

3. Monopulse Based on 4D Antenna Array

3.1. Basic Theory. In theory, the contradiction between the angle measurement precision and large field-of-view exists in any phase-comparison monopulses. To solve this problem, the monopulse technique is combined with the 4D antenna arrays. 4D antenna arrays have been used to generate multiple beams [12, 23], and, more importantly, these beams are formed at different sidebands and point in different directions. Inspired by this unique feature of 4D arrays, a novel phase-comparison monopulse based on a 4D array is presented, as shown in Figure 4. The 8-element 4D arrays are divided into two 4-element subarrays, which are separated by a certain distance $D = 4d = 2\lambda$ (d is supposed to be $\lambda/2$). The two subarrays are excited with the same time sequences, implying that the exciting time sequence of element k ($k = 1, 2, 3, 4$) is the same as that of element $k + 4$. In this way, the power patterns generated by the two subarrays would be the same except for a phase difference, and the received signals of two subarrays, after summed and subtracted with each other, would produce a similar difference-sum ratio K_{4D} as the one shown in Figure 2(d). In order to maximize the signal-to-noise ratio (SNR) of the received signal, a set of band-pass filters can be mounted between the antenna elements and RF switches to filter out the noises outside the center band.

The basic principle of the proposed monopulse system can be stated as follows. Firstly, the large field-of-view is divided into several sectors. Secondly, the multiple beams

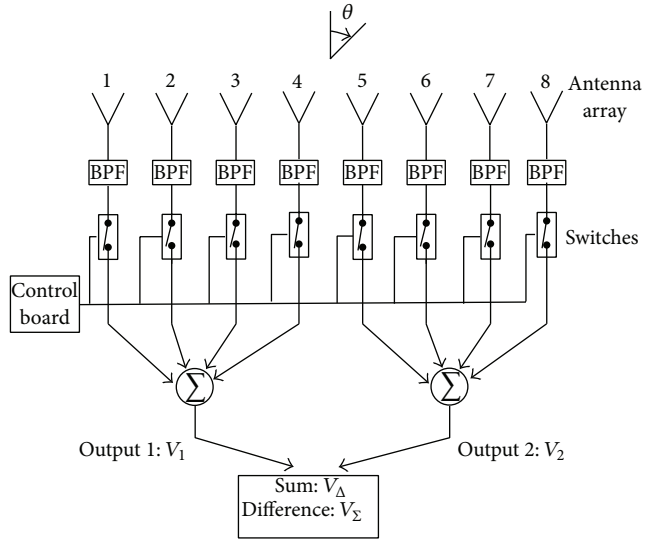

Figure 4: A phase-comparison monopulse system based on an 8-element 4D antenna array.

generated by the 4D array are used to cover these angle sectors, with one beam for one angular sector. Thirdly, the received signals of two identical 4D arrays are phase-compared, and multiple sum-difference patterns are formed with one sum-difference pattern for one sector. These multiple sum-difference patterns are formed at different sidebands with different bore-sight axes and cover the field-of-view as a whole.

Similar to the conventional phase-comparison monopulse, the difference-sum ratio $K_{4D}(m)$ of the 8-element 4D array at the mth sideband can be expressed as

$$\begin{aligned} K_{4D}(m) &= \frac{V_\Delta(m)}{V_\Sigma(m)} \\ &= \frac{\sum_{k=1}^{4} a_{mk} \cdot e^{j(k-1)\beta d \sin\theta}\left(e^{j\beta D \sin\theta} - 1\right)}{\sum_{k=1}^{4} a_{mk} \cdot e^{j(k-1)\beta d \sin\theta}\left(e^{j\beta D \sin\theta} + 1\right)} \\ &= j\tan\left(\frac{\beta D}{2}\sin\theta\right), \end{aligned} \tag{10}$$

where $V_\Delta(m)$ denotes the amplitude of the difference signal at mth sideband, $V_\Sigma(m)$ denotes the amplitude of the sum signal at mth sideband, and a_{mk} is the equivalent complex excitation weighting for the kth element at the mth sideband, calculated by (8). As can be seen, the difference-sum ratio of the 4D array is the same as that of the conventional array, independent of the sideband order m, as shown in Figure 5.

Different from the conventional phase-comparison monopulse, the angle measurement field for the 4D array is divided into several sectors, and each sector is covered by a pair of sum-difference beams. As shown in Figure 5, the angle bearing information can be derived according to the $K_{4D}(m)$ without ambiguity.

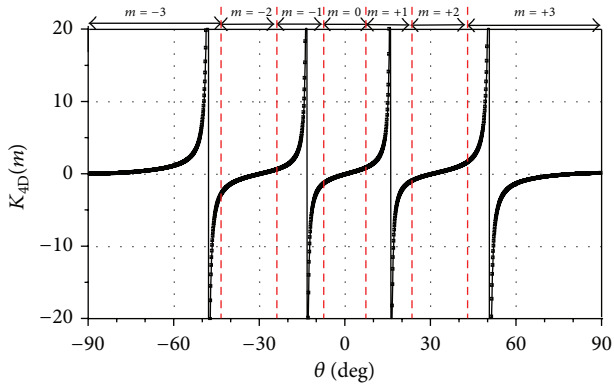

FIGURE 5: Difference-sum ratio K_{4D} of the 4D array where isotropic elements are used. For a signal coming from the mth sector, $K_{4D}(m)$ is used.

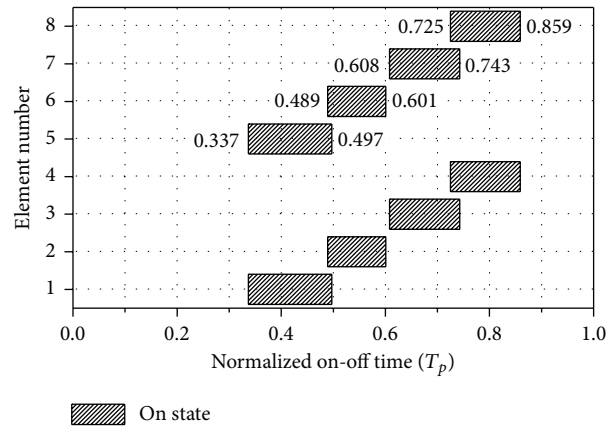

FIGURE 6: The optimized time sequence for the two subarrays.

3.2. Multiple Sum-Difference Pattern Synthesis. In order to steer the multiple beams to the directions of zero and pole points shown in Figure 5, the DE algorithm is used to optimize the time sequence of each subarray. The cost function of the DE algorithm is set as

$$f(X) = w_1 \sum_{m=-3}^{3} \left|\theta^{(m)} - \theta_d^{(m)}\right| + w_2 \sum_{m=-3}^{3} \left|\mathrm{SBL}^{(m)} - \mathrm{SBL}_d^{(m)}\right| + w_3 \sum_{m=-3}^{3} \left|\mathrm{BW}^{(m)} - \mathrm{BW}_d^{(m)}\right|, \quad (11)$$

where the superscript m denotes the sideband number; SBL and SBL_d are the calculated and desired maximum sideband level; θ and θ_d are the calculated and predefined beam direction; BW is the calculated beamwidth and BW_d is the predefined beamwidth to ensure the −3 dB beam crossover level; and w_1, w_2, and w_3 are the corresponding weighting factors for each term. The optimized time sequence is shown in Figure 6, and resulting power patterns of the two subarrays are shown in Figure 7. Note that, in Figure 7, the power patterns of the two subarrays are the same and their phase patterns differ by a phase difference of $\beta D \sin\theta$.

By summing and subtracting the patterns generated by the two subarrays with each other, multiple sum-difference patterns are obtained, as shown in Figure 8. As expected, seven pairs of sum-difference patterns are formed in the direction of $\theta = -48^\circ, -30^\circ, -14^\circ, 0^\circ, 14^\circ, 30^\circ$, and 48°, with each sum-difference pattern covering a sector of the overall field-of-view and the overall field-of-view is extended to $\pm 60^\circ$.

3.3. Method for Direction Finding. Suppose that a signal impinges on the 4D array. The signal will be received by the two subarrays. The spectra of the two received signals can be computed using the fast Fourier transform (FFT) algorithm and their spectra response is then examined. The sideband that has the maximum response provides a rough estimation

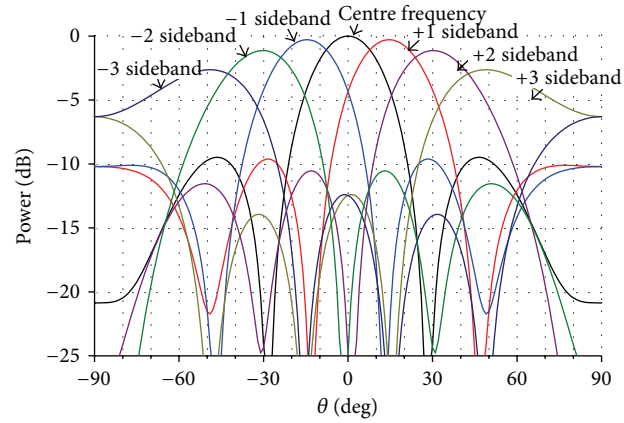

FIGURE 7: The multiple beams generated by subarray 1 and subarray 2 at different sidebands with different pointing directions.

of signal direction. Then sum and subtract the two received signals with each other and compute the spectra of the sum and difference signals. By comparing the amplitude of the difference signal with that of the sum signal, the difference-sum ratio K_{4D} can be obtained, and thus the direction of the signal can be easily determined. A detailed example for direction finding will be presented in the next part.

4. Experimental Setup and Results

4.1. Experimental Setup. To validate the theory presented above, an experiment is conducted in an anechoic chamber. The block diagram of the experimental setup is shown in Figure 9. A horn operating at the frequency of 2.6 GHz is used as the transmitting antenna and is kept in a fixed position. The 4D array composed of an 8-element printed dipole and the feeding network is used as the receiving antenna and is placed on a rotating platform. The feeding network includes 8 SPST switches, two combiners, and a CPLD board that controls the on-off state of the switches. The time sequence shown in Figure 6 is programmed into the CPLD board, which is used to generate the repetition pulse signal to drive the switches. The time modulation frequency is set to be $f_p = 100$ KHz.

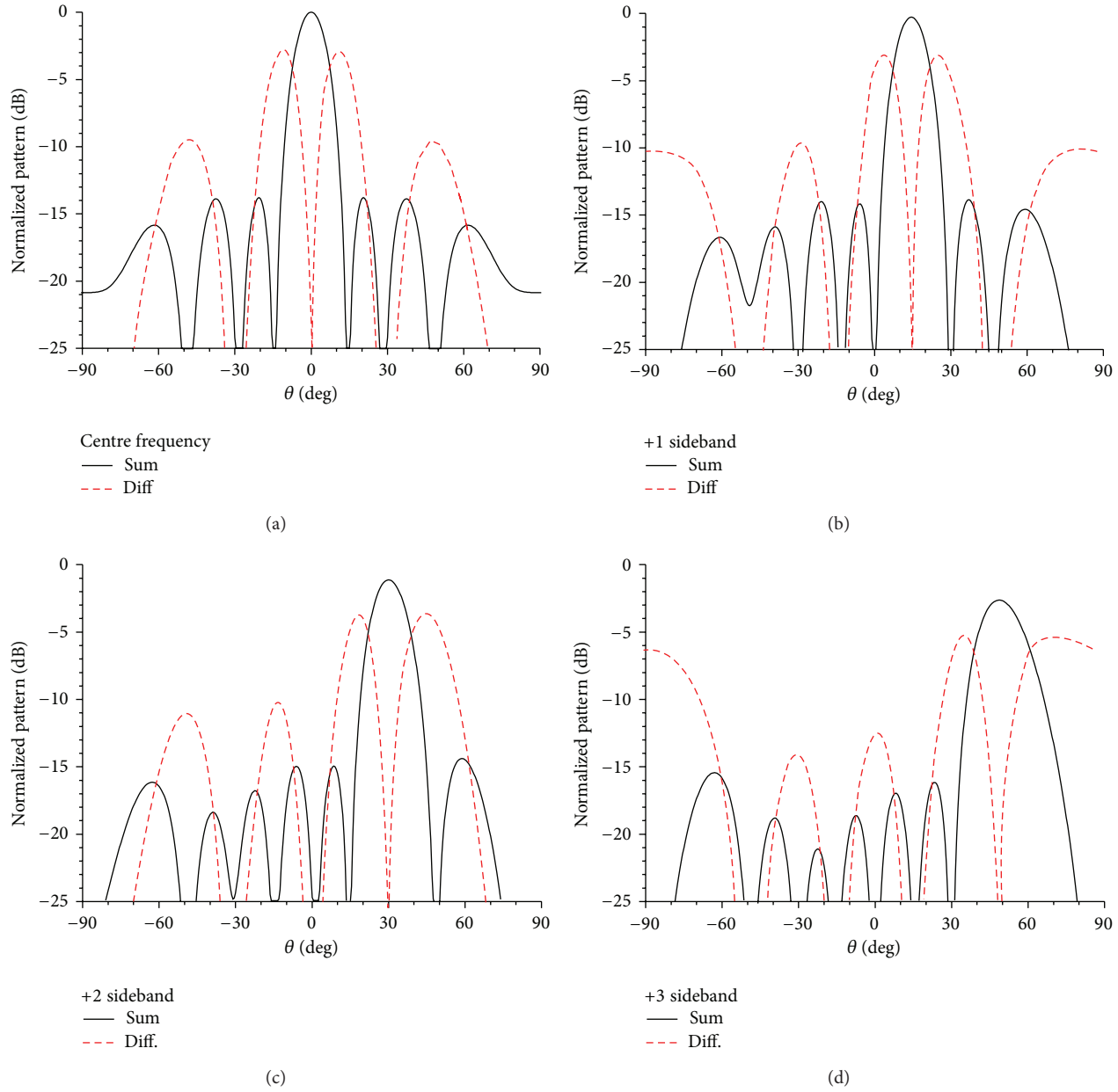

FIGURE 8: The sum-difference patterns formed at different sidebands and different pointing directions by phase-comparing the multibeams of subarray 1 and subarray 2 (only the positive sidebands are shown).

The two antennas are separated with a distance of 14 m to ensure that the far-field testing condition is satisfied. A sinusoid signal of 2.6 GHz is sent to the horn antenna and transmitted. The signal is received by the elements, time-modulated by RF switches, and then summed into two channels by the two combiners. The signals of the two channels are sampled by a digital oscilloscope synchronously. The oscilloscope works at a sampling rate of 20 Gpts/s, which is 7 times higher than the highest frequency of the transmitted signal and satisfies the sampling theorem. Ten periods of the received signals can be stored. The stored signals are then exported to the personal computer (PC) and postprocessed in Matlab afterwards.

4.2. Calibration of Difference-Sum Ratio K. In the theoretical analysis in Parts II and III, isotropic element patterns are used, and the patterns of the two subarrays are the same except for a phase difference. In experiment, the mutual coupling effects, ground plane, and assembly errors affect the arrays' patterns, and the patterns of the two subarrays are not the same any more.

For accurate angle measurement, the active element patterns of the dipole array are firstly measured without time modulation. The active element pattern is the radiation pattern of an element when it is located in the array with other elements matched perfectly [24], taking into account the effect of mutual coupling between array elements. The active

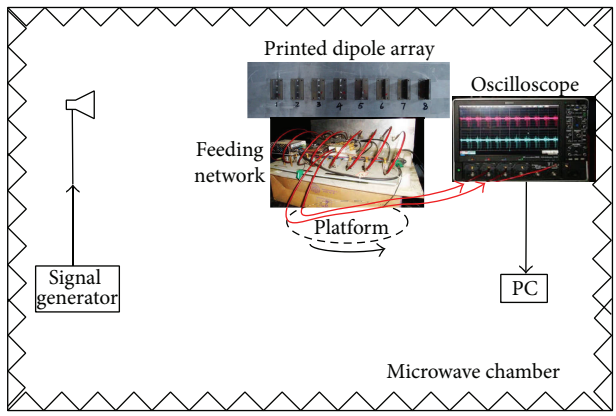

FIGURE 9: Block diagram of the experiment setup.

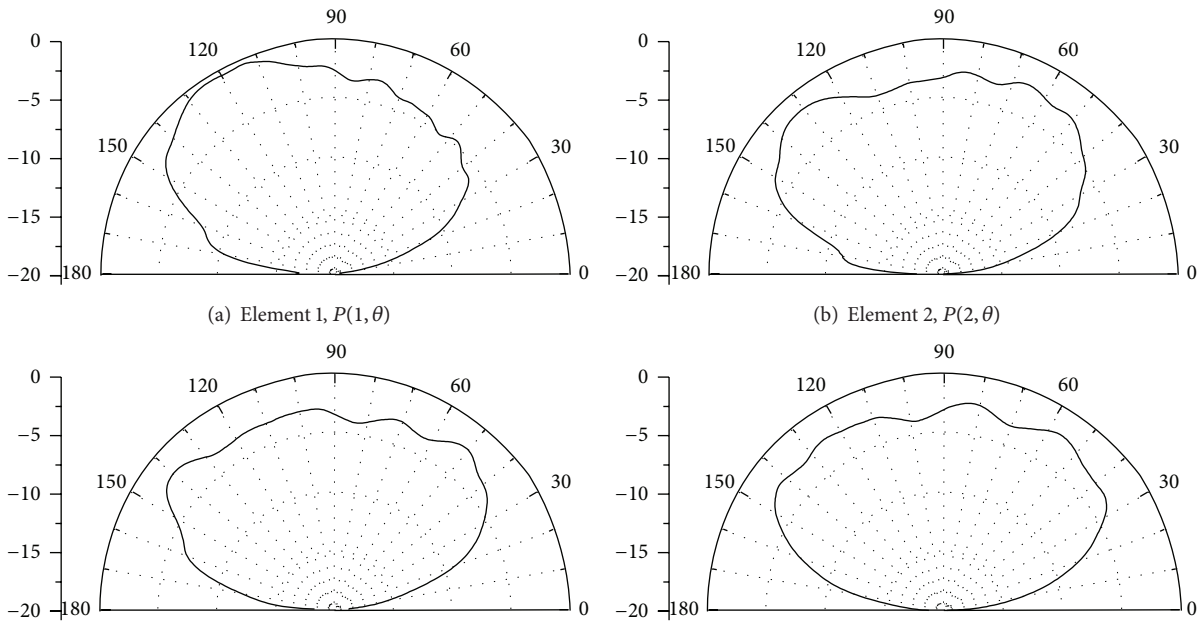

(a) Element 1, $P(1,\theta)$

(b) Element 2, $P(2,\theta)$

(c) Element 3, $P(3,\theta)$

(d) Element 4, $P(4,\theta)$

FIGURE 10: Measured normalized active element amplitude patterns of subarray 1 [denoted as $P(k,\theta)$].

element pattern in the H plane for the azimuth angle from -90° to 90° of each element is measured, and the patterns of element number 1 to number 4 are shown in Figure 10. As can be seen, these patterns are different due to mutual coupling effect, the ground plane, and so forth.

Based on the measured active element patterns, the sum-difference pattern at each sideband can be calibrated and calculated by

$$P_{\text{sum}}(m) = \sum_{k=5}^{8} a_{mk} P(k,\theta) + \sum_{k=1}^{4} a_{mk} P(k,\theta),$$
$$P_{\text{diff}}(m) = \sum_{k=5}^{8} a_{mk} P(k,\theta) - \sum_{k=1}^{4} a_{mk} P(k,\theta), \quad (12)$$

where $P_{\text{sum}}(m)$ and $P_{\text{diff}}(m)$ denote the sum and difference pattern at the mth sideband and $P(k,\theta)$ denotes the active element pattern of the kth element, which is shown in Figure 10. In calculation, both amplitude and phase information are taken into account. Figure 11 shows the calibrated sum-difference pattern at $m = 0, +1, +2$, and $+3$ sideband. As compared to the patterns in Figure 8 where isotropic patterns are used, the calibrated multiple beams of the 7 pairs of sum-difference patterns still point in the directions of $\theta = -48^\circ$, -30°, -14°, 0°, 14°, 30°, and 48°, but the patterns change more or less.

The difference-sum ratio $K_{4D}(m)$ can also be calibrated by comparing the amplitude of the difference pattern with that of the sum pattern, given by

$$K_{4D}(m) = \frac{P_{\text{diff}}(m)}{P_{\text{sum}}(m)}. \quad (13)$$

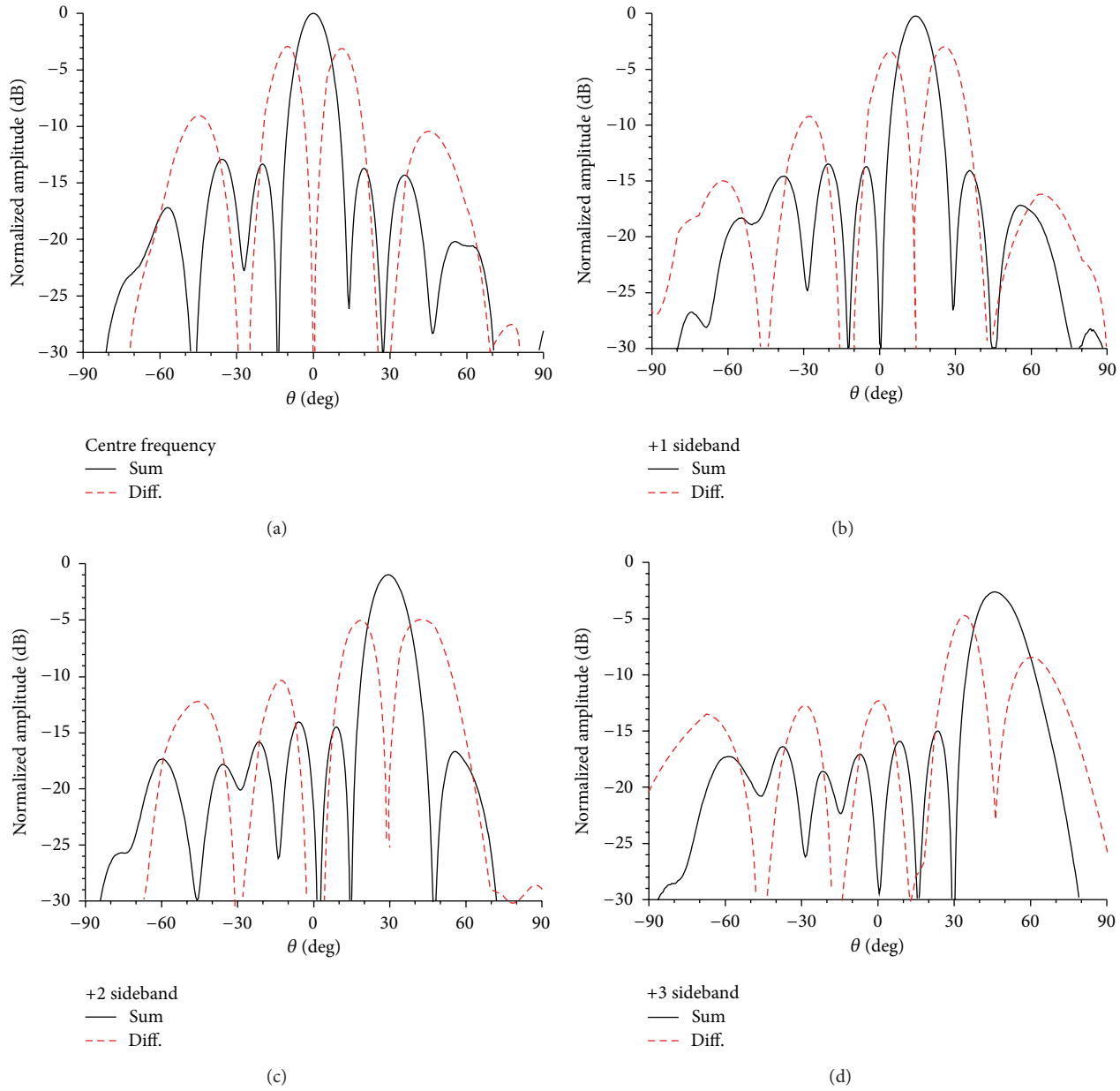

Figure 11: Sum-difference patterns taking into account the measured active element patterns.

Figure 12 shows the calibrated $K_{4D}(m)$ for different sideband signals. As can be seen, the $K_{4D}(m)$ at different sideband are not the same any more. For a signal coming from different directions, the corresponding $K_{4D}(m)$ can be used. For instance, for a signal coming from 30°, $K_{4D}(2)$ should be utilized, since the signal is located in the beamwidth of the sum beam at the +2nd sideband (from 24° to 42°).

4.3. Direction Determination of Signals. Since the horn as the transmitted antenna is at a fixed position, the 4D array is rotated every 5° from −65° to 65° to simulate the situation where the signal comes from a spatial angle. To extract the angle bearing information of the transmitted signal, the exported signals are processed in the following way, as shown in Figure 13.

Firstly, the received signals of subarray 1 or subarray 2 are spectrum analyzed using the FFT algorithm. The sideband that has the maximum response indicates the sector of the field-of-view that the signal comes from and provides a coarse estimation of the arrival direction. The number of the sideband having the maximum amplitude response is designated as M. Secondly, the received signals of subarray 1 and subarray 2 are summed up and subtracted with each other. The resulting sum and difference signals are also spectrum analyzed using the FFT algorithm. The magnitude of the Mth sideband of the difference signal is compared with that of the sum signal, and the difference-sum ratio $K_{4D}(M)$ is obtained.

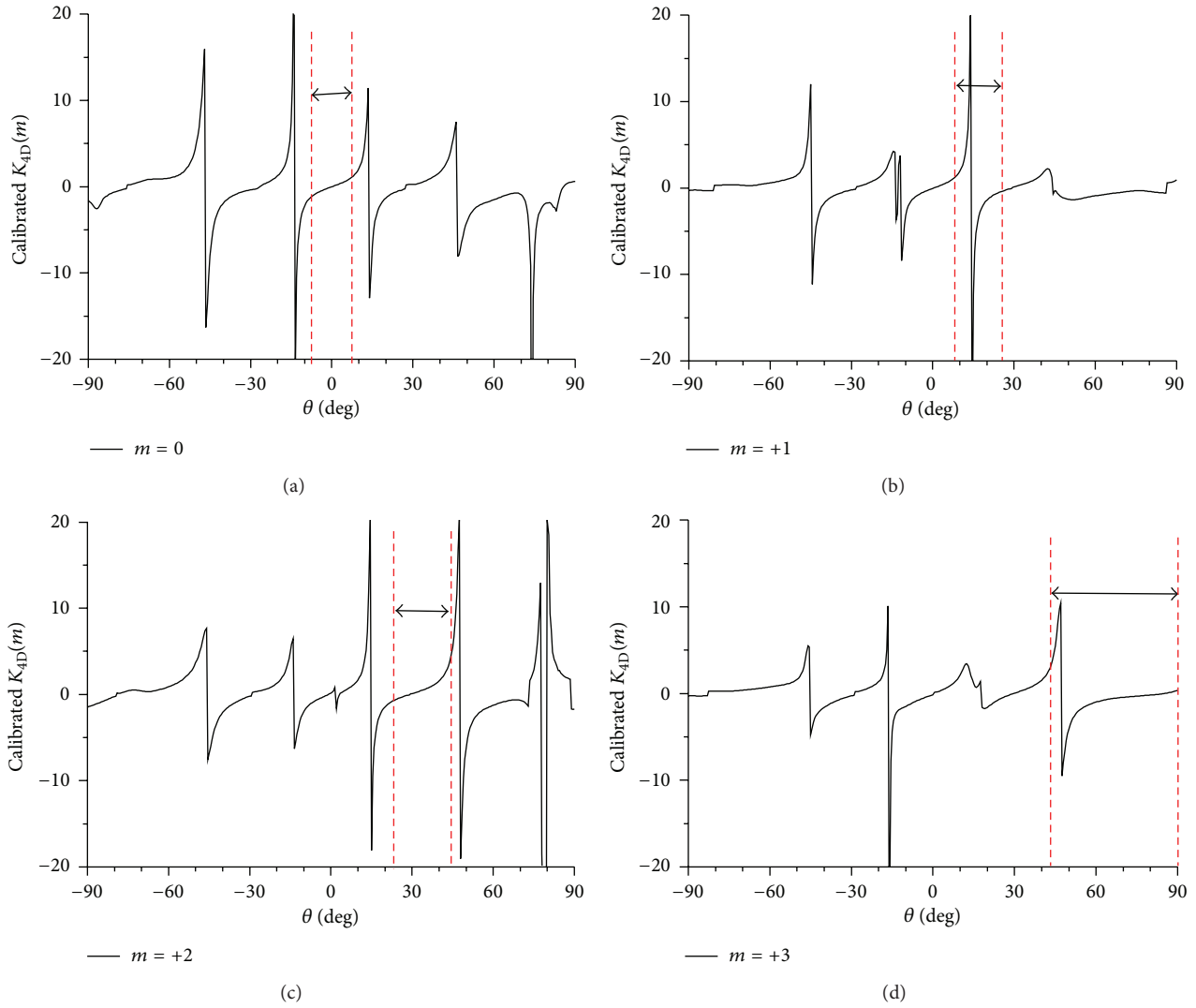

FIGURE 12: Calibrated difference-sum ratio $K_{4D}(m)$ based on measured active element patterns.

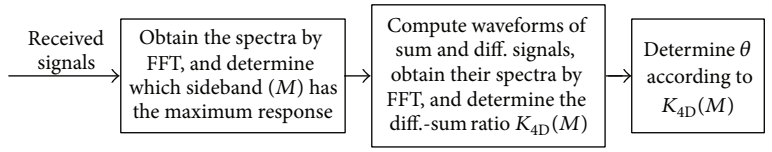

FIGURE 13: Signal processing steps in the 4D array for direction finding.

Finally, the bearing angle can be precisely determined from obtained difference-sum ratio $K_{4D}(M)$, according to the sum-difference patterns of the Mth sideband shown in Figure 12.

Take the case where the transmitter is in the 30° direction as an example. The waveforms of the two received signals of subarray 1 and subarray 2 are shown in Figure 14(a), and their corresponding spectra are shown in Figure 14(b). In Figure 14(b), the maximum amplitude response appears in the +2nd sideband, which indicates that the wave comes from the sector around $\theta = 30^\circ$ and the difference-sum ratio $K_{4D}(2)$ should be chosen as a reference. By summing and subtracting the received signals of subarray 1 and subarray 2, the waveforms of the sum and difference signals are obtained, as shown in Figure 15(a). By FFT, the corresponding spectra of the sum and difference signals are obtained and shown in Figure 15(b). By comparing the amplitude of the +2nd sideband of the difference signal with that of the +2nd sideband of the sum signal, the ratio is found to be equal to +0.137. By looking up the difference-sum ratio $K_{4D}(2)$ shown in Figure 12, the ratio +0.137 corresponds to a wave coming from the direction of $\theta = 30.5^\circ$; thus the measurement error is 0.5°.

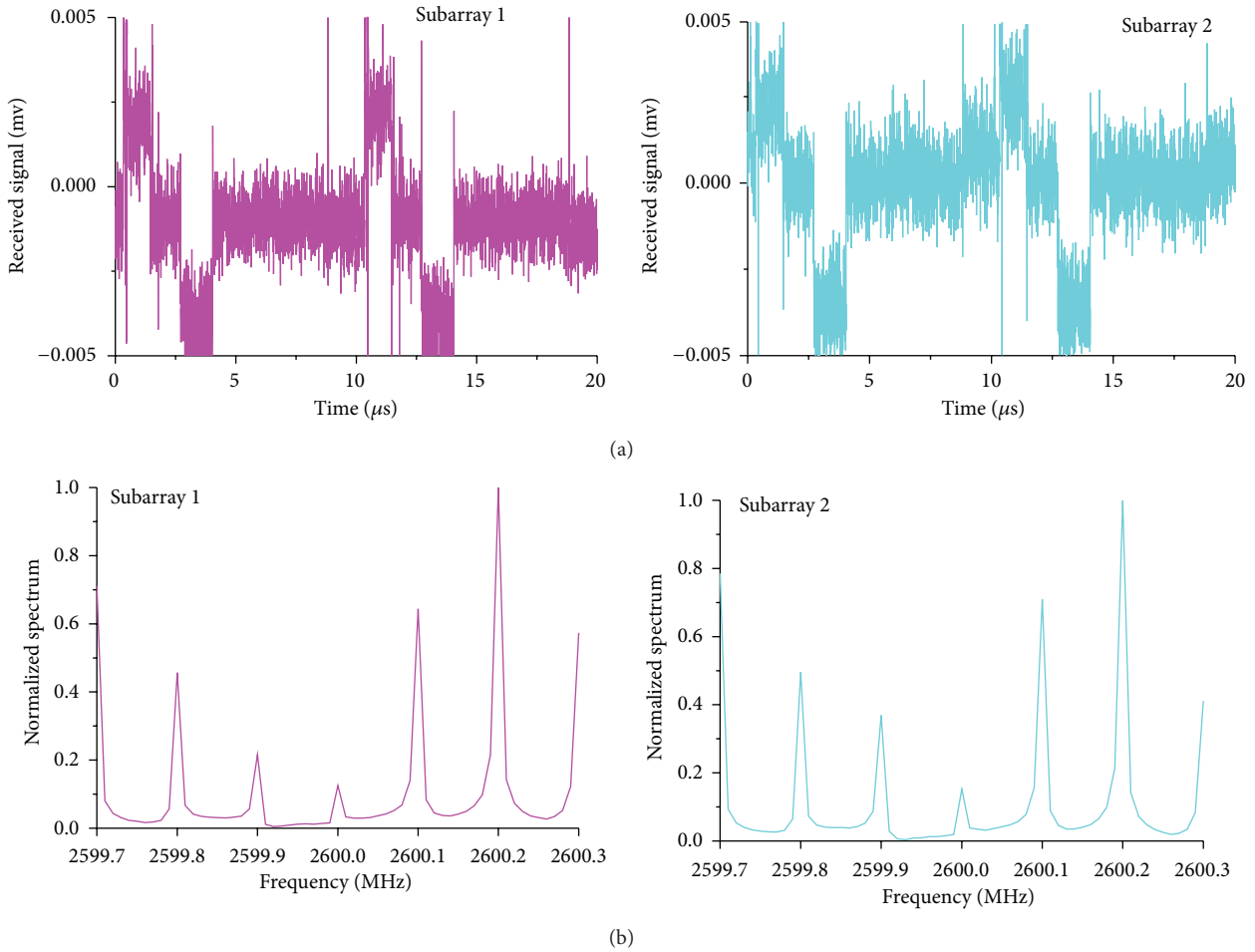

FIGURE 14: The procedure to determine the pair of sum-difference patterns that has the maximum amplitude response and should be used for angle measurement. (a) The waveforms of signals received by the two subarrays at $\theta = 30^{\circ}$. (b) The spectra of received signals received at $\theta = 30^{\circ}$, which are obtained by FFT performed in PC.

The measurement error for a spatial field of $\pm 65^{\circ}$ is shown in Figure 16. For the wave coming from the direction of -60° to 60°, the measurement error is less than 2°. The error is caused mainly by phase imbalance within the two channels and also related to the SNR of the received signal. As a set of suitable BPFs are not available and not used in the experiment, the SNRs of the received signals are not high enough, especially for the signals from the edges of the field-of-view. The SNR of the received signal decreases with the increase of θ. The lower the SNR is, the greater the measurement error will be. In order to provide higher estimation accuracy, more careful calibrations are also needed.

5. Conclusions and Discussions

The 4D antenna array is demonstrated for the application of direction finding over a wide field-of-view in this paper. The time modulation technique in 4D arrays is used to generate multiple beams at different sidebands and the phase-comparison monopulse is used to generate the sum-difference patterns. As a result, multiple pairs of sum-difference patterns with different pointing directions are formed at different sidebands. According to the theoretical analysis, an experimental system is set up and the angle measurement algorithm is calibrated taking into account the active element patterns. The experimental results show that this novel monopulse system provides unambiguous direction finding over a spatial field-of-view of $\pm 60^{\circ}$ with very low computational complexity.

The advantage of the proposed technique is that it can achieve direction finding over a much wider field-of-view by adding a set of RF switches to a conventional array. However, the low SNR performance of the received signals in 4D arrays increases the measurement errors. In order to realize a SNR equivalent to that of a conventional array, a set of BPFs must be added after the elements to filter out the noise outside the center band and avoid the aliasing effect, when the bandwidth of the incoming signal is wider than the modulation frequency. The SNR performance of the 4D array will be reported in the future.

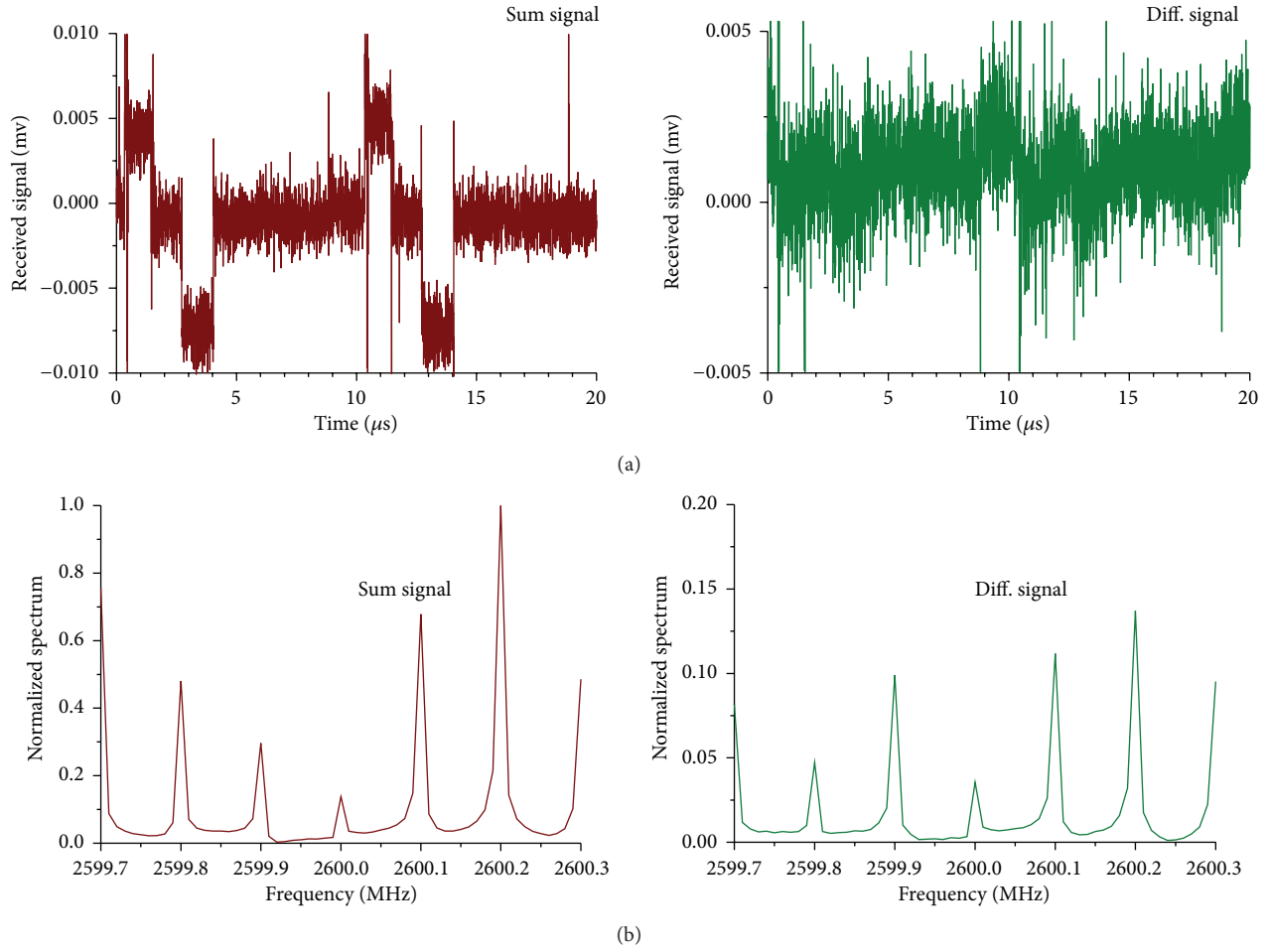

FIGURE 15: The procedure to obtain the difference-sum ratio K: (a) waveforms of sum and difference signals at $\theta = 30^\circ$ and (b) spectra of sum and difference signals at $\theta = 30^\circ$.

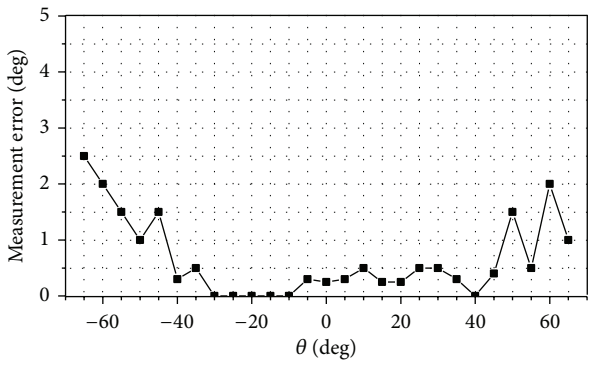

FIGURE 16: Measured estimation errors for a spatial field of ±65°.

Conflict of Interests

The authors declare that there is no conflict of interests regarding the publication of this paper.

Acknowledgments

This work was supported by the Natural Science Foundation of China (Grant no. 61125104) and in part by the 111 Project of China (Grant no. B07046).

References

[1] S. M. Sherman and D. K. Barton, *Monopulse Principles and Techniques*, Artech House, Boston, Mass, USA, 2011.

[2] W. B. Kendall, "Unambiguous accuracy of an interferometer angle-measuring system," *IEEE Transactions on Space Electronics and Telemetry*, vol. 11, no. 2, pp. 62–70, 1965.

[3] L. G. Bullock, G. R. Oeh, and J. J. Sparagna, "An analysis of wide-band microwave monopulse direction-finding techniques," *IEEE Transactions on Aerospace and Electronic Systems*, vol. 7, no. 1, pp. 188–203, 1971.

[4] E. Jacobs and E. W. Ralston, "Ambiguity resolution in interferometry," *IEEE Transactions on Aerospace and Electronic Systems*, vol. 17, no. 6, pp. 766–780, 1981.

[5] H. E. Shanks and R. W. Bickmore, "Four-dimensional electromagnetic radiators," *Canadian Journal of Physics*, vol. 37, no. 3, pp. 263–275, 1959.

[6] W. H. Kummer, A. T. Villeneuve, T. S. Fong, and F. G. Terrio, "Ultra-low sidelobes from time-modulated arrays," *IEEE Transactions on Antennas and Propagation*, vol. 11, pp. 633–639, 1963.

[7] S. Yang, Y. B. Gan, and A. Qing, "Sideband suppression in time-modulated linear arrays by the differential evolution algorithm," *IEEE Antennas and Wireless Propagation Letters*, vol. 1, pp. 173–175, 2002.

[8] S. Yang, Y. B. Gan, A. Qing, and P. K. Tan, "Design of a uniform amplitude time modulated linear array with optimized time sequences," *IEEE Transactions on Antennas and Propagation*, vol. 53, no. 7, pp. 2337–2339, 2005.

[9] S. Pal, S. Das, and A. Basak, "Design of time-modulated linear arrays with a multi-objective optimization approach," *Progress in Electromagnetics Research B*, no. 23, pp. 83–107, 2010.

[10] L. Poli, P. Rocca, L. Manica, and A. Massa, "Time modulated planar arrays—analysis and optimisation of the sideband radiations," *IET Microwaves, Antennas and Propagation*, vol. 4, no. 9, pp. 1165–1171, 2010.

[11] L. Poli, P. Rocca, and A. Massa, "Sideband radiation reduction exploiting pattern multiplication in directive time-modulated linear arrays," *IET Microwaves, Antennas and Propagation*, vol. 6, no. 2, pp. 214–222, 2012.

[12] L. Poli, P. Rocca, G. Oliveri, and A. Massa, "Harmonic beamforming in time-modulated linear arrays," *IEEE Transactions on Antennas and Propagation*, vol. 59, no. 7, pp. 2538–2545, 2011.

[13] Y. Tong and A. Tennant, "A two-channel time modulated linear array with adaptive beamforming," *IEEE Transactions on Antennas and Propagation*, vol. 60, no. 1, pp. 141–147, 2012.

[14] A. Tennant and B. Chambers, "A two-element time-modulated array with direction-finding properties," *IEEE Antennas and Wireless Propagation Letters*, vol. 6, pp. 64–65, 2007.

[15] A. Tennant, "Experimental two-element time-modulated direction finding array," *IEEE Transactions on Antennas and Propagation*, vol. 58, no. 3, pp. 986–988, 2010.

[16] J. Fondevila, J. C. Brégains, F. Ares, and E. Moreno, "Application of time modulation in the synthesis of sum and difference patterns by using linear arrays," *Microwave and Optical Technology Letters*, vol. 48, no. 5, pp. 829–832, 2006.

[17] P. Rocca, L. Manica, L. Poli, and A. Massa, "Synthesis of compromise sum-difference arrays through time-modulation," *IET Radar, Sonar and Navigation*, vol. 3, no. 6, pp. 630–637, 2009.

[18] Y. Chen, S. Yang, and Z. Nie, "Design of a novel monopulse antenna system using the time-modulated antenna arrays," *International Journal of RF and Microwave Computer-Aided Engineering*, vol. 20, no. 2, pp. 163–169, 2010.

[19] P. Rocca, L. Manica, L. Poli, and A. Massa, "Synthesis of compromise sum-difference arrays through time-modulation," *IET Radar, Sonar and Navigation*, vol. 3, no. 6, pp. 630–637, 2009.

[20] X. Huang, S. Yang, G. Li, and Z. Nie, "A novel application for sum-difference pattern detection of signal direction using time-modulated linear arrays," in *Proceedings of the 18th International Symposium on Intelligent Signal Processing and Communication Systems (ISPACS '10)*, Chengdu, China, December 2010.

[21] Q. Zhu, S. Yang, R. Yao, M. Huang, and Z. Nie, "Unified time and frequency domain study of time modulated arrays," *IEEE Transactions on Aerospace and Electronic Systems*, vol. 61, no. 6, pp. 3069–3076, 2013.

[22] L. Poli, P. Rocca, L. Manica, and A. Massa, "Pattern synthesis in time-modulated linear arrays through pulse shifting," *IET Microwaves, Antennas and Propagation*, vol. 4, no. 9, pp. 1157–1164, 2010.

[23] Y. Tong and A. Tennant, "Simultaneous control of sidelobe level and harmonic beam steering in time-modulated linear arrays," *Electronics Letters*, vol. 46, no. 3, pp. 200–202, 2010.

[24] D. M. Pozar, "Active element pattern," *IEEE Transactions on Antennas and Propagation*, vol. 42, no. 8, pp. 1176–1178, 1994.